Graphene-based transparent conductive electrodes for GaN-based light emitting diodes: challenges and countermeasures

Liancheng Wang[1,2*], Yiyun Zhang[2,4], Zi-Hui Zhang[1], Wei Liu[1], Swee Tiam Tan[1], Xiaoyan Yi[2], Guohong Wang[2*], Xiaowei Sun[1*], Hongwei Zhu[3*], Hilmi Volkan Demir[1*]

[1]Luminous! Centre of Excellence for Semiconductor Lighting and Displays, School of Electrical and Electronic Engineering, Nanyang Technological University, 639798 Singapore

[2]Semiconductor Lighting Technology Research and Development Center, Institute of Semiconductors, Chinese Academy of Sciences, Beijing 100083, China

[3]School of Materials Science and Engineering, Center for Nano and Micro Mechanics (CNMM), Tsinghua University, Beijing 100084, China

[4]Department of Electrical and Electronic Engineering, the University of Hong Kong, Hong Kong, China

Emails: Guohong Wang: ghwang@semi.ac.cn; Hongwei Zhu: hongweizhu@tsinghua.edu.cn; Xiaowei Sun: EXWSun@ntu.edu.sg; Hilmi Volkan Demir: volkan@stanfordalumni.org.

KEYWORDS: Graphene; light emitting diodes; transparent conductive electrodes; Gallium Nitride; Chemical Vapor deposition.

Abstract

Graphene, with attractive electrical, optical, mechanical and thermal properties is considered to be an ideal candidate for transparent conductive electrodes (TCEs) in many optoelectronic devices, including III-nitride based devices. However, high contact resistivity (ρ_c) between graphene and GaN (especially p-GaN) has become a major challenge for graphene TCEs utilization in GaN-based light-emitting diodes

(LEDs). Here, we analyzed the graphene/GaN contact junction in detail and reviewed the current research progress for reducing ρ_c in graphene TCEs on GaN LEDs, including interface engineering, chemical doping and tunnel junction design. We also analyzed the current diffusion length for a single layer graphene (SLG) and multiple layer graphene (MLG) TCEs. Finally, to improve the fabrication process compatibility and simplicity with paramount reproduction, a method of directly growing graphene films on GaN by chemical vapor deposition is proposed. We also give a short analysis on the reliability of graphene TCEs for GaN-based LEDs. It is believed that this is the ultimate solution for graphene TCEs application for GaN-based LEDs and other in general for other opto- and electrical devices.

1 Introduction

Thanks to their high efficiency, tiny volume, environmental friendliness and long lifespan, GaN-based light-emitting diodes (LEDs) have recently been investigated extensively [1-3]. LEDs find versatile use in general lighting and illumination, information displays, sensors and visible communications. The state of the art conventional lateral LEDs (L-LEDs) are commonly epitaxially grown on insulating sapphire substrates, typically consisting of u-GaN(~3μm), n-GaN(~3-4μm), InGaN(~2nm)/ GaN(~8-12nm) multiple quantum wells (MQWs), and p-GaN layer (~100-200nm) sequentially. After mesa photolithography and dry etching down to the n-GaN layer, cathode and anode metal contacts will be deposited onto the n-GaN and the p-GaN layers, respectively, from which electrons and holes are injected and recombined within the MQWs. However, restricted by the poor conductance of the p-GaN ($p\sim10^{17}/cm^3$), transparent conductive electrodes (TCEs) with both high optical transmittance and excellent conductance are indispensable to spread the injection current away from the metal pads and avoid additional optical absorption to improve

the light extraction as much as possible[4].

For vertical LEDs (V-LEDs)[5], fabricated through sapphire removal and new metal standing substrate electroplating, the injection current also tends to crowd under the n-type metal electrodes, especially under high injection current density, leading to a serious decline in luminous efficiency[6]. Excellent TCEs are also necessary for achieving high-performance V-LEDs[7]. Conventional indium tin oxides (ITO) TCEs are widely used in touch sensors, flat panel displays, solar cells and GaN-based LEDs. With great advantages as TCEs, ITO has a low sheet resistance of less than 100 Ω, high optical transparency of ~90%, and unlimited scalability. However, ITO is also criticized for its high-cost, poor transparency in the near ultraviolet and ultraviolet ranges, instability in the presence of acids or alkalis, and susceptibility to ion diffusion into the substrate. What is more, for some flexible devices, ITO is fragile and thus easy to crack during twisting and folding, resulting in the failure of the devices. Moreover, ITO cannot withstand the high temperature procedures, which also limits its application to some extent. Due to these limitations, other novel TCEs are extensively investigated. Graphene, a two-dimensional (2D) material, emerges as an ideal candidate with great potential to replace traditional TCEs and has received great research in recent years[8-12]. The outstanding electrical (with reported electron mobility values (μ_n) in excess of 15,000 $cm^2 \cdot V^{-1} \cdot s$), optical (with 97.7% transmittance for monolayer and absorption saturation), thermal (with near-room temperature thermal conductivity between $(4.84 \pm 0.44) \times 10^3$ to $(5.30 \pm 0.48) \times 10^3$ $W \cdot m^{-1} \cdot K^{-1}$), mechanical and chemical properties[12] of graphene make it most attractive and ideal for application as TCEs.

In this article, we first have a brief introduction about the electronic and optical properties of graphene. In the following we reviewed and summarized research

progress, current related approaches and developments from both our and other groups for graphene TCEs utilized in GaN-based LEDs. More detail will be introduced on our tunnel junction design to reduce the ρ_c between p-GaN and graphene. For simplifying the fabrication process and improving the adhesion of graphene, we also give a review on graphene local growth on GaN so far. Through our analysis, we think this is the ultimate solution to overcome the fabrication compatibility and adhesion problem, which paves the way for the ultimate application of graphene TCEs on GaN-based LEDs.

1.1 Electronic and optical properties of graphene

Graphene is a single planar sheet of sp^2 bonded hybrid carbon atoms with s, p_x and p_y atomic orbitals on each carbon atom forming three strong σ bonds with other neighboring atoms. The remaining p_z orbital of each carbon atom produces a filled band of π orbital (valence band) and an empty band of π^* orbital (conduction band) [13, 14]. The electronic wave-functions from different atoms overlap, except for the p_z (π) orbital and the others, p_x and p_y atomic orbitals-the overlap is strictly zero due to symmetry. Consequently, the p_z electrons formed π orbitals can be treated independently and with this π-band approximation, the dispersion relations E (k_x, k_y) can be easily obtained[15]:

$$E^{\pm}(k_x, k_y) = \pm\gamma_0\sqrt{1+4\cos\frac{\sqrt{3}k_x a}{2}\cos\frac{k_y a}{2}+4\cos^2\frac{k_y a}{2}} \qquad (1.1)$$

where $a=\sqrt{3}a_{cc}$, a_{cc} =1.44Å being the carbon-carbon lattice distance and γ_0 is the transfer integral between the first-neighbor π orbitals. The k= (k_x, k_y) represents the ensemble of the available electronic momenta in the first Brillouin zone. The valence band and conduction band touch at the six two-dimensional hexagonal Brillouin corners (Dirac points, K), making graphene a semi-metal or zero-gap semiconductor.

Expanding equation (1.1) for low energies near the K points yields the linear dispersion relationship:

$$E(k) = \pm \hbar V_F |k| \quad (1.2)$$

Where k=K'-K, is measured from the Dirac points and v_F (~10^6 m/s) is the electron group velocity. Fig. 1(a) shows the band structure of graphene (left) and the zoom-in of the energy bands close to one of the Dirac points (right)[14]. The semimetal behavior and massless Dirac fermions characteristics of graphene revealed by the band structure shown in Fig. 1(a) theoretically ensure its superior electrical, optical and thermal properties, such as high carrier mobility, almost wavelength-independent and saturable optical absorption, etc. Fig. 1(b1) shows the transmittances of single layer (SLG) (~97.7%) and bilayer graphene (~95.4%)[16]. A. K. Geim et.al[16] found that the opacity of a SLG is defined solely by a series of fundamental constants: fine structure constant $\alpha = \frac{e^2}{\hbar c} \approx \frac{1}{137}$ (where c is the speed of light), and physically describes coupling between light and relativistic electrons:

$$T_{SLG} = (1 + 0.5\pi\alpha)^{-2} \approx 1 - \pi\alpha = 97.7\% \quad (1.3)$$

Additionally, graphene only reflects <0.1% of the incident light in the visible region, and this reflectance reaches only to ~2% for ten layers. The transmittance of MLG is linearly proportional to the layer number n:

$$T_{MLG} = 1 - nA_{SLG} = 1 - 2.3\% \cdot n \quad (1.4)$$

Where A_{SLG} represents the absorption of each layer, with A_{SLG}=1-T=1-97.7%=2.3% over the visible spectrum. MLG can be optically equivalent to simple stack of SLG, with little perturbation of each adjacent layer. What is more, graphene shows a quite flat absorption spectrum over a very wide region (400-2500nm) and saturation absorption characteristics when the input optical intensity is above a threshold value

(Fig. 1(b2) [16]). Inset of Fig. 1(b2) shows the transmittances of white light as a function of the number of graphene layers[16].

2 Current approaches for graphene TCEs utilization in LEDs

2.1 The state-of-the-art of graphene TCEs: Various approaches have been explored to obtain graphene-based TCEs, including: micromechanical cleavage[17], CVD growth on metal substrate[18-22], chemical reduction of graphene oxide[23, 24], spaying[25], dip[26], spin coating[27], vacuum filtration[28] and role-to-roll processing[29]. Considerable progress has been made since the first attempt to produce graphene-oxide-based TCEs. Gilje[25] et al. decreased R_s from 40GΩ/sq to 4MΩ/sq following reduction with dimethylhydrazine. Graphitization, hydrazine exposure and low temperature annealing, or high-temperature vacuum annealing further decreased R_s down to 800 Ω/sq for T=82%. Kostya S. Novoselov et al.[17] reported graphene TCEs prepared by micromechanical cleavage with T≈ 98% and R_s =400 Ω /sq using a layer of polyvinyl alcohol to induce n-type doping. TCEs have been produced using the ultra-large graphene oxide sheets that are deposited layer-by-layer on a substrate using the Langmuir Blodgett (LB) assembly technique developed by Jang-Kyo Kim's group[30].

After thermal reduction and chemical doping, R_s of 500 Ω /sq and T of 90% have been obtained. By intercalating micromechanical cleavage obtained MLG with $FeCl_3$, R_s of 8.8 Ω/sq and T of 84% have been obtained by Monica F. Craciun group[31]. Sukang Bae[29] *et. al* reported the roll-to-roll production and wet-chemical doping of predominant monolayer 30-inch graphene films grown by chemical vapor deposition (CVD) onto flexible Cu substrates, reaching a low R_s of 125 Ω/sq and T of 97.4%. Fig. 1(c) is a summary for graphene TCEs R_s and T reported from different groups. It shows that graphene TCEs derived from the CVD method (especially on Cu), combined with doping could outperform the conventional ITO TCEs. What is more,

as we know, T is dominated by the layer number (n) of graphene, with T= 1- nπα, where $\pi\alpha \approx 2.3\%$ is the absorption for a single layer. It seems the "trade-off" rule that the lower sheet resistance will naturally come with the higher opacity (corresponding to larger n) also works for graphene TCEs. However, for the-state-of-art of CVD grown and transferred graphene TCEs, defects (such as dislocations, steps and grain boundaries) formed during CVD process, and disruptions (such as wrinkles, cracks and edges) formed during the transfer process, can effectively scatter the charge carriers, leading to the degradation of the transport properties of graphene and lower electrical conductivity[32]. By making efforts to bring down the defects during growth and transfer, or by healing the defects through metal nanowires, graphene conductivity can be further improved while keeping its optical transparency[33]. Note that graphene TCEs mentioned and discussed later on in this paper are grown by the CVD method, except where specially clarified.

To function perfectly as TCEs, besides the high T and low R_s as mentioned above, there are several other requirements including strong adhesion and good ohmic contact to the target substrate. When graphene is transferred onto GaN LEDs, we need to guarantee that the electrons can effectively transport from graphene into GaN, which means the electrons can transport across the p-GaN/graphene (L-LEDs) or u-, n-GaN/graphene (V-LEDs) hetero-junction with resistance as low as possible. However, due to the large work function (W_F) mismatch between graphene (~4.8eV for weak p-doped) and p-GaN (~7.5eV), u-, n-GaN (~4.0eV), the high interface contact barrier (Ψ_b) would hinder the movement of carries (electrons or holes） and increase the R_c, leading to the higher operating voltage (V_F) of LEDs ultimately. And this large ρ_c value at GaN/graphene, especially for p-GaN/graphene junction, indeed has become the most challenging obstacle for graphene TCEs application on GaN-

based LEDs. Further, consider the compatibility of graphene in LEDs' fabrication processes, the poor adhesion between graphene and GaN poses another unavoidable and critical problem, and severely affects the LED reliability.

2.2 Metal-graphene contact

Figs. 2(a1) and (b1) show the schematic drawings of L-LEDs and V-LEDs incorporating graphene TCEs. Figs. 2(a2) and (b2) show the corresponding emission micrograph images of L-LEDs and V-LEDs. Fabricating LED devices with graphene TCEs will essentially involve making metals contacts. Therefore, before introducing graphene TCEs contact with GaN in GaN LEDs, it is necessary and prudent to better understand the contact properties between metal and graphene.

2.2.1 Graphene-metal contacts category: Due to the vanishing density of states (DOS) approaching the Dirac points, even a small amount transfer of electrons will shift the Fermi level (E_F) significantly ($\Delta E_F=W_M-W_G=0.47$eV when 0.01 electrons transferred). Intuitively one could assume that an electron is transferred into (withdrawn from) graphene when $W_G>W_M$ ($W_G<W_M$), and $\Delta E_F=0$ when $W_G=W_M$. However, G. Giovannetti [34] *et al.* found that the crossover point lies at $W_M-W_G=0.9$eV. Through further first-principle calculations at the level of density function theory (DFT), they stated that metals can be divided into two classes. Qiushi Ran [35]further states that the projected DOS of the metal's d-orbital dominates the formation of physical/chemical contact. Chan *et al.* [36] states that contacts between group I-III metal atoms and graphene are ionic, while the transition metals make covalent bonds with graphene. Therefore, graphene-metal contacts can be divided into two classes (Table.1(a)): chemisorbed graphene-metal contacts such as graphene-Ti, Co, Ni, Pd, with an equilibrium separation d_{eq}~2Å, in which the graphene bands are strongly perturbed and will acquire a mixed graphene-metal character; physical absorbed

graphene-metal contacts such as graphene-Al, Cu, Ag, Au, Pt, with an equilibrium separation d_{eq}>3.2Å, in which graphene retains its unique bands characteristics with metal physically contacted.

2.2.2 Graphene-metal contacts resistivity: On the other hand, reported values of metal-graphene ρ_c vary and appear to depend on the metal used, fabrication procedure, gate bias, measurement conditions and even metal microstructure: a gate-dependant ρ_c of 500 Ωμm of Ni-graphene at 300K, 700±500 Ω μm for Ti-graphene[37], 185±20Ωμm at 300K and 120±20μm at 6K[38] and ~5×10^{-6} Ω cm^2 for Ni-graphene using the cross-bridge Kelvin structure[39]. Fengnian Xia[40] used Landauer's approach [$G= (4e^2/h)TM$, where M is the number of the conduction mode in graphene, T is the transmission probability] to understand metal-graphene ρ_c, and mechanisms such as charge transfer [34, 41, 42], gate dependence of the Dirac point energy, broadening of DOS (as electron-hole puddle formation) and carriers tunnel probability as a function of the interfacial potential barrier width, shape and height are considered. Xiang Ji[43] further considered the Fermi velocity difference of graphene under and away from metal. In GaN LEDs, metal systems usually contain Ni/Au, Cr/Pt/Au, Al/Ti/Au or Ti/Al/Ti/Au. Metal-graphene ρ_c are in the range of 10^{-5}-10^{-6}Ωcm^2, according to the reports mentioned above and our group[37-39, 66].The corresponding voltage drop can be negligible, which is calculated to be ~0.01V at 1A forward operating current for a 320 ×320 μm^2 contact ($\Delta V=IR=I\rho_c/S=1A\times10^{-5}\Omega cm^2/10^{-3}cm^2$). The interfacial metal Ni, Ti and Al belong to the chemical and physical contact class respectively, according to ref. 34.

Attributed to the fact that Cr has a half-filled 3d-electron shell ([Cr]$3d^5 4s^1$), the most stable configuration (along with full filling $3d^{10}$), Cr/graphene should be physical contact type. Generally, graphene TCEs cover the whole chip and the area

ratio between metal and graphene is ~10%, as can be seen from Fig. 2(a1) and (b1). Nevertheless, this metal-graphene contact can be still evaluated using Fengnian Xia's modified Landauer model[40]. According to above discussion, the chemisorbed metal would distort the band structure of graphene and the physical absorbed metal has negligible influence on that. This metal induced variation on graphene would thus have an effect on graphene/GaN contact properties. However, in all the published articles related to graphene TCEs in GaN LEDs, the influences of metal on graphene-GaN contact are neglected. Understanding the interplay of metal-graphene-GaN is inspiring and of great significance. Further, the principle for metal/graphene contact is actually similar with graphene CVD growth on metal, so understanding this can also help to reveal the mechanism of CVD graphene growth on different metal substrates. This is beneficial for understanding graphene local growth on GaN substrate, which will be discussed later in this article.

2.3 GaN/graphene contact

It is important to understand the graphene/GaN interface physics and transport mechanism for carriers transporting across it. The S. Tongay group[44, 45], the Haijian Zhong group[46] and our group[47] have obtained the Schottky barrier height (Ψ_b) by fitting graphene-GaN I-V curve using thermionic emission theory, i.e., the Richardson equation:

$$I = AA^{*}T^{2}\exp(-q\psi_b / kT)[\exp[\frac{q(V-IR_s)}{nkT}-1] \quad (2.1)$$

Where A is the contact area, A*is the Richardson constant (26.4 $Acm^{-2}K^{-2}$ for n-GaN and 96.1$Acm^{-2}K^{-2}$ for p-GaN), R_s is the series resistance and *n* is the ideality factor. Taking Ψ_b, R_s and *n* as fitting parameters, Ψ_{bp} and Ψ_{bn} can be statistically determined. Table. 1(b) summarizes the obtained Ψ_b by different groups as mentioned above. Ψ_b for graphene/Si, GaAs junctions were also listed as reference. Superscript T, F and X

for Ψ_b denote theoretically calculated, I-V fitted and XPS test results, respectively. Ψ_b^T was simply estimated based on the difference between W_F (G) and χ.

Haijian Zhong[46] and our group's results[47] unambiguously show that Ψ_b^F is rather lower than Ψ_b^T. However, S. Tongay's [44] results show comparable value between $\Psi_{b,n}^T$ and $\Psi_{b,n}^{F,}$ yet they did not provide $\Psi_{b,p}^F$ results, making comparison incomplete. Like the graphene/metal contact, electrons transferred into (out of) graphene, raise up (brings down) the E_F of graphene when it contacts with n-GaN (p-GaN), leading to a lower $\Psi_{b,n}^F$ ($\Psi_{b,p}^F$). Haijian Zhong[46] claimed this self-adaptive shift of E_F in graphene to be the dominant reason accounting for the differentiation between Ψ_b^T and Ψ_b^F. XPS tests have been further carried out by our group[47] and the corresponding Ψ_b^X values were also listed in Table. 1(b). Ψ_b^X falls in between Ψ_b^T and Ψ_b^F, especially $\Psi_{b,p}^X$ (2.08eV) is significantly higher than $\Psi_{b,p}^F$(0.49eV). We think Ψ_b^X most closely approaches the real Ψ_b.

2.3.1 Understanding the discrepancy between Ψ_b^T and Ψ_b^X: First, we assume the aforementioned self-adaptive-E_F-shift in graphene to be the sole reason contributing to the discrepancy between Ψ_b^T and Ψ_b^X. Figs. 2(c1) and 2(c2) show sketches of the graphene/p-GaN junction before and after alignment, with $\Delta W_{Gra}=W_{Gra}^*- W_{Gra}$ equal to the variation of graphene work function due to self-adaptive effect. Here, electrons transferred out of graphene lead to $E_{F,G}$ being reduced,. We denote $N_{transferred}$, $\Delta E_{F,G,}$ to be the number of the transferred electrons per unit area, shifted E_F,

$$\Delta E_{F,G} = -sign(N_{transfered})\sqrt{2N_{transfered}/(q^3 D_0)} \qquad (2.2)$$

$$N_{transfered} = \sqrt{2q\xi_r\xi_0 N^* V_{D,p\_GaN}} \qquad (2.3)$$

$$eV_{D,p\_GaN} + \chi = \varphi_{b,p} \;;\; \chi = e(E_{F,p\_GaN} - E_{V,p\_GaN}) = k_b T In(N_v / p) \quad (2.4)$$

Where equation (2.2) is obtained by integrating the linear DOS, D_0=0.09 eV^2 per unit

cell for E within 1eV of the conical points. It is well known that the Schottky barrier values are well described using either Bardeen or Schottky limits. Many experiments have demonstrated that the ionic wide gap semiconductors SiC and GaN are managed by Schottky-Mott (S-M) limit [48-50]. Hence, the graphene/GaN interfacial states are neglected in our model, in contrast with Haijian Zhong's model. $\Delta E_{F,G}$ is first assumed to be equal to 0.62eV (Ψ_b^T- Ψ_b^X=2.7eV-2.08 eV). $V_{D,\,p\text{-}GaN}$ can be derived from Eqs. (2.2) and (2.3), finally the $\Psi_{b,p}$ value can be obtained from Eqn. (2.4). Finally, the $N_{transferred}$ value obtained from Eqs. (2.3) is$2.394*10^{13}cm^{-2}$ and $\Psi_{b,p}$ to be ~0.36 eV (assuming E_F-E_v=0.13eV), which is significantly lower than $\Psi_{b,\,p}^X$ (2.08eV).

It is noteworthy that the above calculations are based on a simple self-adaptive model. There are several possible reasons accounting for the discrepancy between $\Psi_{b,\,p}^X$ and $\Psi_{b,\,p}^T$. First, $E_{F,\,G}$ may lie far away from (typically below) the Dirac point before graphene contacts with GaN. The deviation can be attributed to hole doping of the graphene during the Fe(III)NO_3 etching-transfer process[51, 52]. Therefore, instead of Eqs. (2.2) and (2.3), $N_{transferred}$ should be modified as in the following,

$$\Delta E_{F,G} = \left| E_{F,G} - E^0{}_{F,G} \right| \qquad (2.5)$$

$$E^0{}_{F,G} = -\hbar \left| v_F \right| k_{F0} = -\hbar \left| v_F \right| \sqrt{\pi N_0} \qquad (2.6)$$

$$E_{F,G} = -\hbar \left| v_F \right| k_F = -\hbar \left| v_F \right| \sqrt{\pi (N_0 + N_{transfered})} \qquad (2.7)$$

where $\hbar$ =6.5×10^{-16} eVs, v_F is the Fermi velocity of ~1.1×10^8cm/s and $E_{F,G0}$ is calculated to be 0.287eV below the Dirac point when $N_0=5\times10^{12}/cm^2$; a shift associated with the aforementioned p-doping during processing. Again it is assumed that, $\Delta E_{F,G}$ to be 0.62eV. Then accordingly, $N_{transferred}$ can be calculated to be ~$4.5\times10^{12}/cm^2$. By substituting $N_{transferred}$ back into Eqs. (2.3) and (2.4), the $\Psi_{b,p}$ value can be calculated to be ~1.18 eV. It is still much lower than $\Psi_{b,\,p}^X$. Except for the $E_{F,\,G}$

divergence, the discrepancy between the calculated $\Psi_{b,p}$ and $\Psi_{b,p}^{X}$ values might also be attributed to: (1) the formation of an interface dipole at the graphene/GaN interface, serving as a plane capacitor (within the bond polarization theory) [53-55].

Cheng Gong[56] *et al.* has proposed the metal/graphene/metal sandwich geometry to strengthen the interface interaction. He suggests that interface charge repulsion occurs, resulting in charge redistribution away from the interface into both metal slabs and within the graphene basal plane. The electron accumulation graphene plane formed allows the antiparallel dipole throughout the interface to interact constructively in the parallel alignment due to the alternative reservoirs of the opposite charges. Considering the metal/graphene/GaN sandwich structure (even graphene is partly covered by metal), a more complex charge redistribution phenomenon may happen; (2) according to G. Giovannetti's work [34], the top metal Cr may interrupt the intrinsic π band structure of graphene by internal chemisorption. All these will have an impact on the equilibrium band alignment, and thus Ψ_b.

2.3.2 Understanding the discrepancy between Ψ_b^F and Ψ_b^X: Let us recall I-V test and have a comparison between Ψ_b^F and Ψ_b^X. Generally, there are several mechanisms accounting for the carriers transporting across the GaN/graphene interface: thermal emission-diffusion and tunnel[57,58], with its correspondent current denoted as $I_{TE,D}$ and I_T, respectively. Fig. 2 (d1) and (d2) show the schematic band structures and carriers transportation when graphene contacts with p-GaN and n-GaN. We attribute the discrepancy between Ψ_b^F and Ψ_b^X to the carrier tunnel transport component, whose flow path is in parallel with the thermal emission-diffusion component ($I_{TE,D}$) and was totally neglected in Eqn. (2.1). So the obtained I is actually the sum of I_T and $I_{TE,D}$, and Ψ_b^F obtained from the I-V fitting is actually a counterfeit barrier height.

Tunnel probability is related to the density of defects and dislocations located

in the interface or space charge zone, acting as the multiple tunnel paths for carrier transport[59, 60]. Due to the lattice mismatch of epitaxial GaN on sapphire (~16%), high-density dislocations (~10^8/cm^2) makes I_T even become dominant on GaN based contact. Referring to S. Tongay' work [45], we noticed that it is commercial n-type GaN they used, which usually demonstrate a lower dislocation density than that of GaN epitaxial layer on sapphire. This of course will bring down I_T and the obtained Ψ_b^F value approaches our Ψ_b^X value. Refer to graphene/n-Si Schottky solar cells, which have been successfully demonstrated by our group[12, 61, 62]. The Schottky barrier height has been derived to be ~0.78eV from I-V fitting, in agreement with the theoretically predicted Ψ_b^T(=W_G-χ=4.8 eV-4.05 eV =0.75eV). Low I_T and high $I_{TE,D}$ is one of the prerequisites for solar cells working. In the purest crystalline Si (with the lowest defect density) junction the carrier tunnel is inhibited which is just opposite to the case of graphene/GaN contact where I_T is dominant. Temperature-dependent I-V characteristics from our group[47] and the S. Chandramohan group[63] further confirm the existence of I_T the component in graphene/GaN contact. Next we turn our attention to the effect of bias on $W_{F,G}$[64], and thus on Ψ_b^F. Unlike conventional metals, graphene's work function $W_{F,G}$ is a function of bias and the SBH value and does not stay constant. For graphene/n-GaN junction, when forward (reverse) bias is applied the graphene will be positively (negatively) charged. Correspondingly $E_{F,G}$ will decrease (increase), $W_{F,G}$ will increase (decrease), causing Ψ_b to increase (decrease). The fixed SBH assumption during the I-V fitting no longer holds. This is similar to the aforementioned self-adaptive effect. Typically the reverse biased voltage is much larger compared with the forward bias, usually leading to significantly reduction in Ψ_b. S. Tongay[44] *et.al* has observed the non-saturating reverse current in graphene-semiconductor junctions, but not in graphite and metal-based Schottky junctions, due

to the fixed Fermi level of the latter.

2.3.3 Experimentally derived Graphene/GaN contact resistivity: The p- and n-GaN/graphene junctions are both reverse biased when LEDs are operated at forward bias. It is meaningful to know the specific R_c values of contact between graphene and different GaN (n-GaN, u-GaN, p-GaN), as for different LED structures, graphene films were deposited on the GaN surfaces with different doping types, concentrations and polarities. We have used a conventional circular transmission line method (CTLM) to obtain ρ_c [65, 66]. Although the charge transfer doping effect and other possible band variations in metal/graphene/GaN system are inevitable and there is complexity inferred from our discussion in metal/graphene contact, we still can first overlook these factors in ρ_c calculation. After dissolving the metal substrate and transferring the CVD-grown graphene onto the GaN surface, metal Cr/Pt/Au with a CTLM pattern was deposited. The CTLM patterns consist of 100 μm^2 ohmic pads with gap spacing of 10, 20, 30, 40, 50 and 60 μm. By reasonable and rational approximation, ρ_c values of graphene/Cr, p-GaN, u-GaN, n-GaN, N-polar u-GaN, N-polar n-GaN are fitted and calculated to be ~0.9×10^{-5}, ~4.3×10^{-1}, ~3×10^{-2}, ~1.1×10^{-5}, ~2.4×10^{-2} and ~$0.9\times10^{-6}\Omega cm^2$. It can be concluded that, in case of a given graphene, ρ_c values of graphene/GaN contacts are mainly determined by W_F gap and carrier concentration of GaN; that is to say, a lower W_F mismatch and a higher carrier concentration will lead to lower ρ_c. Various defects and impurities could be generated during LLO (laser lift off) and ICP (Inductively Coupled Plasma) processes in N-polar GaN fabrication process[67], we think this could bring down the ρ_c values for graphene/N-polar GaN contact. Huei-Min Huang [68] *et. al* found that the MQWs-covered graphene can screen of the polarization field in the c-plane GaN-based quantum well. This would have a negligible effect on graphene/GaN contact, however.

2.4 Graphene on conventional lateral LEDs

Gunho Jo[69] *et. al* first demonstrated MLG TCEs in blue LEDs. The MLG-TCEs LED shows V_F (~5.6 V@20 mA) and 37% lower light output power (LOP), compared ITO TCEs LED (~3.8 V@20 mA). Tae Hoon Seo[70] et al. demonstrate a graphene TCEs LED exhibits ~25% improved LOP and increased V_F to 5.87 V from 3.4V compared to the ITO TCEs LED, respectively. Byung-Jae Kim[71-73]first attempted incorporating graphene TCEs in ultra-violet (UV) LEDs, which exhibited significantly high V_F(26.5V@1mA). Even though benefiting from the aforementioned self-adaptive, tunnel and electrical doing effects, R_c, the value of graphene/p-GaN contacts is still too large. Taking ρ_c to be $4.3\times10^{-1}\Omega.cm^2$ (as calculated above) and the contact area S (almost equal to the chip area) to be ~10^{-2} cm^2, the voltage drop across the graphene/p-GaN junction will be ~0.86V and ~15V at 20mA and 350mA forward currents respectively. Here we will summarise the efforts being devoted to ρ_c reduction for graphene TCE applications in conventional lateral LEDs, including approaches such as interface engineering, chemical doping, annealing, etc.

2.4.1 Interface engineering

Through graphene/p-GaN interface engineering to create virtually hybrid graphene, TCEs is one of the most feasible approaches. The design rule is to insert an interlayer sandwiched between graphene and p-GaN, as shown in Fig. 3(a). The interlayer should be transparent, conductive and have low ρ_c with both p-GaN and graphene. The choice of interlayer materials includes: Ni[74], NiO_x[63, 75], ITO[76, 77], ZnO nanorods[78, 79], Ag[80-83], Au nanoparticles[84-86], AgNWs (Ag nanowire), *etc.* Table. 2 list the reported graphene hybrid structure, features and corresponding chip results. The interlayer generally reduces ρ_c and V_F. However, it often reduces the T as well (~10-20% loss after interlayer insertion). Normally, the final graphene hybrid TCEs based

blue LEDs' electrical and optical characteristics lie between that of bare graphene and conventional ITO based blue LEDs. Notably, in the UV region, graphene hybrid TCEs based LEDs beat that of conventional ITO TCEs due to graphene's wavelength-independent transmission even in the UV region.

2.4.2 Chemical doping

Generally speaking, the principle of chemical doping to improve graphene/p-GaN contact is to introduce foreign electron withdrawing agents onto the surface of graphene which leads to p-type doping and thus increases W_F of graphene[29, 87-89], as shown in Fig. 3(b1). Sukang Bae et. al[29, 84-86, 90, 91] have tested various wet doping agents and the results were summarized in Fig. 3(b3). They found that $AuCl_3$ in Nithomethane and HNO_3 are among the most efficient doping agents. Researchers from different groups have demonstrated an improvement of electrical and optical characteristics of blue and near UV LEDs with Au-doped graphene TCE-based LEDs, as can be clearly seen in Table. 3. We also used HNO_3[47, 92] evaporation to dope the graphene TCEs and the experimental set-up is shown in Fig. 3(b2). The p-(n-)GaN/graphene band diagram variation after HNO_3 treatment was also shown in Fig. 2(d1) and (d2) (red line), respectively. Decreased Ψ_b or narrowed space-charge layer will initiate higher percentage of I_T, causing a reduction in ρ_c. Both L- LEDs and V-LEDs (3.17V@350 mA, 3.64V@1000 mA) show decreases in V_F and ~19% enhancement in LOP. Note that doping will decrease the carrier mobility of graphene and the correspondent effect on its conductivity should be checked.

2.5 Current diffusion length (L_s) analysis for graphene TCEs

Taking R_s~1000Ω/sq and ρ_c =1Ωcm^2, current diffusion length L_s in SLG TCEs, can be roughly calculated to be $L_s \approx \sqrt{\rho_c / R_l} = \sqrt{1\Omega \cdot cm^2 / 100\,\Omega} = 316\mu m$. For a

typical interdigital pattered metal contact in 1mm*1mm device, L_s is much larger than the neighbored metal space width (~250μm), indicating that even the R_s of the state-of-the-art SLG is huge, SLG can still efficiently spread the current to achieve uniform distribution thanks to "current blocking effect" of the relatively large "vertical resistance" ρ_c, However, the relatively larger ρ_c would add to the series resistance ($R=R_c/S=1\Omega cm^2/0.01cm^2=100\Omega$) and ultimately increase the device V_F ($\Delta V=RI=100\Omega\times0.35A=35V$).

$$R_s=\frac{\rho}{t}=\frac{1}{nq\mu_n\cdot t}\propto\frac{1}{N^*},\ \rho_c\propto P\propto\exp\left[-\frac{2eV_D}{e\hbar(N^*/m\xi\xi_0)^{1/2}}\right] \quad (2.8)$$

Eqn. (2.8) reveals that both R_s and ρ_c would decrease with electrons transferred out of p-type graphene. Putting the reported value before (R_s~1000Ω/sq and ρ_c=1Ωcm) and after chemical doping ((R_s~300Ω/sq and ρ_c=0.1Ωcm) into above equation, we can obtain the current diffusion length L_s after chemical doping $L_s\approx\sqrt{\rho_c/R_l}=\sqrt{0.1\Omega\cdot cm^2/300\Omega}=182\mu m$. Even though L_s decreased after chemical doping in this case however, the contact resistance also decreased ($R=\rho_c/S=0.1\Omega cm^2/0.01cm^2=10\Omega$) so the ultimately increased device V_F is comparably small ($\Delta V=RI=3.5V$)

As the SLG R_s after chemical doping is still too large, multilayer graphene (MLG) are also under investigation as an alternative. Surveying the MLG TCE from a bird's-eye view, taken R_s~30Ω/sq and $\rho_c=0.01\Omega cm^2$, the current diffusion length L_s is determined to be 182μm, the same order with that of chemical doped SLG. The introduced series resistance was greatly decreased ($R=\rho_c/S=0.01\Omega cm^2/0.01cm^2=1\Omega$), despite at the cost of the optical transparency (T=1-2.3% n, n is the MLG layer number). We can further understand the current flow in MLG as a resistor network (Fig. S1). In-plane conductivity (σ-xy) and the out-of-plane conductivity of MLG (σ-z)

are assumed to be constant, and all of the current is injected into the top film. We have neglected the fact that the in-plane resistivity of the bottom layer has been reported to be larger due to the effects of the charged impurities in the substrate. L_s and L_z represent the distance that the current flow in plane and out of plane, before homogeneously distributed. Taking L_s minimum to be 150μm, and the interlayer separation of MLG to be a_0=0.34nm, for L_s »4.5×10^5 (=150μm/0.34nm) L_z, MLG exhibits the same sheet conductance regardless of the number of stacked layers because of the poor interlayer conductivity (i.e., all of current flows in the top layer, path I); for L_s «4.5×10^5 L_z, increasing the layer number adds conductive channels in parallel therefore resulting in a decrease in R_s that is inversely proportional to the number of MLG (path II); for L_s ~4.5×10^5 L_z, R_s saturates after a certain number of layers. L_s/L_z ratio can be estimated in terms of in-plane conductivity (σ-xy) and the out-of-plane conductivity (σ-z), which is as high as ~9×10^4 [32,33]. This indicates that stacking graphene layers essentially adds channels for charge transport and saturates after a certain number. To achieve a current diffusion length of ~150μm, MLG layer number can be estimated to be 5~6 (1.50×10^5nm/0.34nm*n=9×10^4). In a real VLEDs device (Fig.5(b)), the n-GaN layer actually serves as the additional intrinsic TCE, so the layer number of the ideal MLG TCEs n should less than 5. Further chemical doping of MLG should further decrease R_s and ρ_c.

2.6 V-LEDs and others

We are the first to transfer graphene TCEs onto the N-polar u-GaN surface of V-LEDs[93]. All of the graphene TCEs-based V-LEDs chips shows improved LOP and the average increase is about 25%. However, due to the relatively large R_c between graphene and u-GaN, V_F (4.19V@350mA) degrades compared with the control sample (3.96V@350mA). By dry etching N-polar n-GaN, combining with graphene

TCEs and a HRM CBL (high reflective membrane current blocking layer) deposited on the p-GaN side, we can manipulate the current distribution and obtain the best chip results[92], which shows 60% increase in LOP and relieved EQE droop compared with control sample. Relying on its low flexural rigidity, graphene also was used as stretchable transparent interconnections in micro-scale LEDs and V-LEDs arrays[94, 95]. It can conform itself to corrugated and even bending surface, in a manner yielding intense physical contact and thus low R_c and good reliability. We have reported the in-situ fabrication of bendable micro-scale hexagonal pyramids array V-LEDs with graphene as stretchable electrical interconnects[95]. Under tensile strain while bending, the adjacent graphene sheets slide against each other, hence the tensile strain can be easily "absorbed and cancelled". What is more, graphene can be buried during CVD process, serving as quasi-nucleation layer[96], thermal dissipation layer[97] and transfer sacrificial layer[98].

3 Proposals

Even though the state-of-the-art interface engineering or chemical doping have been proved to be useful to addressing the high ρ_c problem for graphene TCEs on GaN LEDs several obvious limitations of these methods can be observed: 1.Add much more fabrication complexity, especially for the interface engineering method; 2. Generally, the above-mentioned $AuCl_3$ or HNO_3 treatment is surface doping (chemical doping includes surface transfer doping and substitutional doping), which does not modify the bulk structure and could be reversible. It also means that the doping agents can be desorbed from graphene, leading to the doping process malfunctioning. Annealing proves to be efficient to reduce ρ_c to some extent[63, 99], yet it has its own limitations. Here we demonstrate our two proposals for graphene TCEs' utilization.

3.1 Tunnel junction (TJ) approach

The TJ approach introduces single or multiple n-doped $In_xGa_{1-x}N$ layers on the top of p-GaN layer during local MOCVD growth and replaces additional deposition steps during chip processing before graphene transferring, as illustrated in Fig. 4(a) and the sketched graphene-n-$In_xGa_{1-x}N$/p-GaN band diagram in Fig. 4(b). Two TJ interfaces therefore include graphene/n-$In_xGa_{1-x}N$ interface and n-$In_xGa_{1-x}N$/p-GaN interface. An anomalous nearly ohmic (linear) current-voltage characteristic has been observed by Esaki[100] in the reverse biased TJ junction, which first revealed the quantum tunnel across the depletion region of the junction. Tunnel resistance (TR) is determined by the equivalent energy and momentum states of the electrons and holes at the both TJ sides and the tunnel distances (TD). Inferred from our calculation of graphene/GaN contacts ρ_c above[66], a lower ρ_c value could be expected between graphene and the top heavy n-doped $In_xGa_{1-x}N$ layer. This is due to the high probability of holes (electrons) tunnel from graphene ($In_xGa_{1-x}N$) to $In_xGa_{1-x}N$ (graphene), which has been described in Fig. 2 (d2). As to the n-$In_xGa_{1-x}N$/p-GaN interface, degenerately doping will bring up E_F into the conduction band (CB). When reverse bias is applied to the n-$In_xGa_{1-x}N$/p-GaN junction (i.e. LED is forward biased), the tunnel probability for holes from valence band (VB) of p-GaN across the TJ junction will increase. Large-density intrinsic dislocations (10^8/cm) and defects in GaN grown on sapphire also provide multiple tunnel paths for carrier transportation. What is more, as p-GaN is grown at a relatively lower temperature (960℃) compared with n-GaN (1050℃), a degraded material quality with higher dislocation density results, which makes it more preferable for carriers to tunnel across. As the n-$In_xGa_{1-x}N$ layer is thinner (2nm) than the total depletion width of the two tunnel junctions, the two TJ interfaces would be connected and the n-$In_xGa_{1-x}N$ layer is totally depleted.

This makes easier for carriers to tunnel across and thus reduces the total series resistance. Although the proposed TJ design principle is simple, to realize TJ with a low TR in epitaxial growth needs effort in both growth parameter optimization and rational TJ structure. For example, because of the ionic component discrepancy in InN and GaN, a space charge will develop at the interface of GaN/InN. Behave the same as doping induced charge, the space charge will bend the TJ bands and reduce the TD, TR. Also the narrower band gap of InN further reduces TD. Interval insertion of $In_xGa_{1-x}N$(x may be not fixed) in the TJ layer will create multiple stairs for holes trespassing[57, 59, 100].

Here we demonstrate proof-of-principle of our first effort for TJ-graphene TCEs for blue LEDs. A 2nm-thick n^+-$In_xGa_{1-x}N$ layer was additionally grown on p^+-GaN, with growth temperature T~744℃. In composition has been designed to be ~0.1(lower than In composition in the MQWs) to prevent the re-absorption of emitted light from MQWs (with In fraction about 15%) in the top TJ layer. Fig. 4(c1) shows the top-view SEM images of LED chip (a) before and (b) after transferring graphene. Fig. 4(c2) shows the I-V curves and I-LOP of LEDs based on conventional ITO, bare graphene and graphene-InGaN TJ TCEs. Graphene-TJ TCEs-based LEDs exhibit lower V_F (3.58V@20mA) and higher LOP (8.18mW), compared with that of bare graphene-based LEDs (5.02V@20mA, ~3.85mW). Though it is still inferior to ITO-based LEDs' performance (3.08V@20mA, ~12.39mW), this preliminary result shows the proposal of TJ TCEs is promising. Further optimized design of the tunnel structures and an improvement in graphene material quality can be beneficial for further enhancement of the graphene TCEs based LED devices performance.

3.2 Graphene local growths on GaN

So far nearly all the graphene TCEs in GaN-based LEDs mentioned above are

derived through the wet-transfer CVD method, with its inherent obvious drawbacks[101]: the transfer process is very complicated and susceptible to unintentional and irreversible doping or contamination, leading to the adsorption/accumulation of residues, oxides and wrinkles at the graphene/GaN interface, and hence greatly affecting the contact properties. Also, it is quite indispensable for graphene to adhere strongly with the target substrate. Steven. P. Koenig[102] found adhesion energy of 0.45±0.02 J m^{-2} for monolayer graphene and 0.31±0.02 J m^{-2} for two-to-five layered sheets. Taeshik Yoon[103] *et Al.* found the adhesion energy of monolayer graphene as grown on copper to be 0.72±0.07 J m^{-2}. Both results suggest ultrastrong adhesion of graphene membranes due to intrinsic graphene mechanical properties and graphene/substrate interface electron redistribution. Indeed, strong adhesion is very important for chip fabrication, performance and reliability. Ideally, for SLG, according to theoretical prediction and experimental results[102, 103], it shows a strong adhesion with the underlying substrate. However, for bilayer graphene and MLG, carbon atoms between the layers that are held together by relatively weak van der Waals forces, thus prone to cleavage, and peeling off together with the top metal contact, even though the bottom layer in bilayer graphene and MLG can adhere strongly to the substrate[102]. However, we found that in our chip fabrication process, graphene is very fragile and extremely prone to be exfoliated or broken, especially in metal lift-off and cleaning processes (Fig. 5(a), exfoliated graphene with PMMA), contrasting with Steven. P. Koenig and Taeshik Yoon's reports. We assume the poor adhesion arises from wet-transfer process. For wet-transferred SLG or MLG, if there are some residues at the bottom, the risk for peeling off of graphene TCEs together with the residue will increase. Further, bearing an unaffordable high consumption of energy and time, the cost of graphene CVD and transfer process is yet to be reduced

to be competitive in widespread applications. It is of great significance to develop a reproductive, reliable and feasible technique to grow graphene directly on the target substrate (as Si, GaN, GaAs etc.). We think this is the ultimate solution for graphene TCEs and widespread applications.

The mechanisms for CVD graphene precipitation have been well understood and verified in many transition metals[20, 104-108] (belonging to the group VIII metals) and catalytic carbides of transition metals[109] (as TaC, WC, TiC, HfC and LaB_3), with Ni and Cu as typical two representatives. For Ni, Ni_3C solid solution is formed at elevated temperature and the solubility decreases while temperature decreases, resulting in the precipitation of carbon into graphene. For Cu, it has very low carbon solubility and just acts as a catalyst. This is attributed to the metal d-orbitals differentiation, surprisingly coinciding with metal/graphene contacts introduced above: partially d-orbitals filled metals (as $Ni3d^84s^2$, $Co3d^74s^2$, $Fe3d^64s^2$) are capable of providing low energy pathways for chemical interaction or appropriate intermediates formation with carbon, both in CVD growth and contact conditions; conversely, metal with full or half filled d-orbitals (as Cu $3d^{10}4s^1$) can only form soft bonds with carbon via charge transfer from d-orbitals to the empty s states, acting as a true catalyst for graphene formation. By placing solid carbon source (PMMA) onto or in between Ni/ insulating substrates, James. M. Ture's group[110, 111] has successfully demonstrated bilayer graphene CVD growth through carbon diffusion out of Ni.

Taking these experiences for CVD graphene on GaN, some critical issues should be addressed. Different to inert insulating substrate, e.g., SiO_2, Si_3N_4, GaN is more likely to decompose at elevated temperature, especially for GaN-based LEDs with InGaN/GaN MQWs; high temperature will lead to In segregation and hence influence the emission properties. C_2H_2, which has a lower decomposition temperature, is

recommended as the carbon precursor, instead of conventional CH_4. Additionally, the mechanism for CVD graphene growth on non-metallic substrates is still obscure, whether it is catalytic or not. Recent advance in graphene grown on non-metallic substrates includes CVD on hafnium dioxide[112, 113] (HfO_2), sapphire[114], SiO_2[115], Si_3N_4[116], BN, MgO[117], and ZnS etc. Jie Sun[114] suggests a non-catalytic self-assembly process of carbon cluster. Andrew Scott[118] emphasizes the importance of step sites of the non-metallic substrates, which anchor the carbon nano-flakes and serve as nucleation sites, resembling the conventional step-flow CVD process.

Based on the experiences both from others and our group, we think graphene CVD on GaN is a combination of catalytic and non-catalytic processes. Fig. 5(b) sketches the growth mechanism of graphene on GaN. MOCVD grown GaN surface is often lack of N atoms and excessive of Ga atoms. The elevated temperature will make the Ga atom more dominant due to GaN decomposition[119]. Inferred from the mechanism of CVD graphene growth on Cu, a metal Ga-with full occupied d-orbital ($3d^{10}4S^{2}4P^{1}$) catalytic process is possible. Actually, Ga and carbon are known to be an insoluble system, similar to Cu (with quite low affinity with carbon), further supporting the above analysis[120, 121]. Although the GaN-graphene bonding type is basically van der Waals adhesion, we believe the interatomic force between GaN and locally grown graphene is stronger than that via wet transfer methods due to a stronger bonding between metal Ga and carbon atoms[103]. What is more, due to the state-of-the–art MOCVD GaN growth (on sapphire substrate) technology and especially the lowered growth temperature of the top p-GaN, the p-GaN surface typically exhibits random distributed hexagonal pits, which serve as the favorable sites for carbon source dissociation and carbon nucleation. However, this also makes the deposited carbon layer not uniform, in contrast with those on inert substrates such

as Si_3N_4 and SiO_2.

Jie Sun[122] has demonstrated the first result of CVD grown large-area carbon thin film on GaN at 950℃ and 750mbar for 5min in a flow of 160sccm C_2H_2 and 1000sccm NH_3. Low decomposition temperature C_2H_2 as the precursor and an overpressure of NH_3 were chosen in order to protect the GaN surface from dissociating. The as-grown film shows ~6.7nm thickness (Fig. 5(c1)) and abnormal ~2% transmittance (Fig. 5(c2)), and is more resistive than expected. Yet the absence of 2d peak in the Raman spectrum (Fig. 5(c3)) and detail refraction TEM results (Fig. 5(b1)) indicate the as-grown film may be a combination of graphene sheets and some other carbon film allotropes. Specifically, for graphene TCEs' application on lateral LEDs, we propose a combination with the TJ scheme: local growth of graphene on n-In_xGaN_{1-x}/p-GaN-MQW-n-GaN layer. This should result a relatively lower contact resistance and strong adhesion simultaneously. Much effort still needs to be devoted for scalable, continuous, uniform and thickness and some other properties (e.g. doping) controllable graphene TCEs deposition directly on GaN-based LEDs. The mechanism should also be deeply understood.

4 Reliability of graphene TCEs for GaN-based LEDs

The reliability of graphene TCEs for GaN-based LEDs undoubtedly needs the equal attention, yet there are few reports on it up to date. Byung-Jae Kim[123] reported the severe degradation of graphene TCEs when the UV LEDs were continuously biased for 30s at a bias of 10V. There was less degradation when the UV-LED was operated at a pulsed bias condition with 5% duty cycle for totally 30s. It indicates that the high junction temperature and joule heating caused oxidation of the graphene TCEs are accountable for its degradation. Li Liu[124] found that the O_2 etching kinetics varies strongly with the number of graphene layers. Oxidation of triple layers is

similar to the natural graphite and HOPG, featured with uniformly sized one layer-deep etch pits, which is initiated at preexisting point defects, followed by constant radial growth. In contrast to the triple layers, SLG and bilayer graphene are more reactive to O_2: featured with one-layer-deep or two-layer-deep etch pits, oxygen-atom attack can nucleate and grow etch pits on even a defect-free basal plane, as well as at preexisting defects. Further refer to the reports of graphene reliability in other devices, such as Field-Effect Transistors (FET)[125-127]and supercapacitors[128,129], the possible degradation mechanism for graphene TCEs in GaN-based LEDs can be: degradation from the graphene itself, the graphene/GaN contacts and GaN/metal contact. The heating and cooling cycles can make graphene TCEs structurally deformed, showing regions of curvature and domains of lower than hexagonal symmetry, resulting in some sp^3 C orbital character and π -orbital misalignment. This is expected to lead to degradation in graphene mobility and significantly increased reactivity with O_2. The generated-heat also accelerates the graphene TCEs' oxidation process, which can severely degrade the graphene and thus LEDs' optical and electrical characteristics[122]. Aging under environmental exposure, intrinsic graphene acoustic phonon scattering, Coulomb impurities, surface roughness and surface polar phonon scattering could leads to mobility degradation of graphene[126]. The interfacial impurity scattering (eg.Mg^{2+} in p-GaN) could degrade the mobility of graphene and graphene/GaN contact resistance[125]. Electromigration (EM) is another issue to be considered. The current-induced thermal annealing make the electrons gain certain energy, atoms become separated from the interface and are transported in the direction of the current. This will increase the metal/GaN contact resistance and even make the graphene TCEs electrical interconnect fail[128].

5 Conclusions

We have presented a review of the state-of-art graphene TCEs used in GaN-based LEDs. The electronic and optical properties of graphene have been reviewed. Graphene/GaN contacts then were analyzed and discussed in detail. Self-adaptive and reverse bias doping of graphene E_F, as well as carriers' tunnel are considered to be responsible for the relatively lower barrier heights of graphene/GaN interface. Current approaches, including interface engineering, chemical doping and tunnel junction design for graphene TCEs utilization in LEDs and correspondent chip results have been summarized. For overcoming the obvious complexity and fragile drawbacks of the wet-etching transfer method, graphene directly grown on GaN by the CVD method was strongly recommended and introduced in detail. Finally, we give a short analysis on the reliability of graphene TCEs for GaN-based LEDs. We think that graphene directly grown on GaN by CVD combined with tunnel junction design could be the ultimate countermeasure to obtain low series resistance (contact resistance included), fabrication compatibility and reliable adhesion, paving the way for the ultimate application of graphene TCEs in GaN-based LEDs and in general of other opto- and electrical devices.

Acknowledgement

This work is supported by the National Research Foundation of Singapore under Grant No.NRF-CRP-6-2010-2, NRF-RF-2009-09, the Singapore Agency for Science, Technology and Research (A*STAR) SERC under Grant No.112 120 2009 and the National High Technology Program of China (Grant No. 2013AA03A101), the National Natural Science Foundation of China (Grant No. 51372133, 61306050 and 61306051).

6 References

1. S. Nakamura, Science **281** (5379), 956-961 (1998).
2. P. Waltereit, O. Brandt, A. Trampert, H. T. Grahn, J. Menniger, M. Ramsteiner, M. Reiche and K.

H. Ploog, Nature **406** (6798), 865-868 (2000).
3. Z. Liu, T. Wei, E. Guo, X. Yi, L. Wang, J. Wang, G. Wang, Y. Shi, I. Ferguson and J. Li, Applied Physics Letters **99** (9), 091104 (2011).
4. J. K. Kim, S. Chhajed, M. F. Schubert, E. F. Schubert, A. J. Fischer, M. H. Crawford, J. Cho, H. Kim and C. Sone, Advanced materials **20** (4), 801-804 (2008).
5. S.-J. Wang, K.-M. Uang, S.-L. Chen, Y.-C. Yang, S.-C. Chang, T.-M. Chen, C.-H. Chen and B.-W. Liou, Applied Physics Letters **87** (1), 011111 (2005).
6. Y. Zhang, H. Zheng, E. Guo, Y. Cheng, J. Ma, L. Wang, Z. Liu, X. Yi, G. Wang and J. Li, Journal of Applied Physics **113** (1), 014502 (2013).
7. D. W. Kim, H. Y. Lee, M. C. Yoo and G. Y. Yeom, Applied Physics Letters **86** (5), 052108 (2005).
8. A. K. Geim and K. S. Novoselov, Nature materials **6** (3), 183-191 (2007).
9. F. Bonaccorso, Z. Sun, T. Hasan and A. C. Ferrari, Nat Photon **4** (9), 611-622 (2010).
10. P. Matyba, H. Yamaguchi, M. Chhowalla, N. D. Robinson and L. Edman, ACS Nano **5** (1), 574-580 (2010).
11. Y.-M. Lin, C. Dimitrakopoulos, K. A. Jenkins, D. B. Farmer, H.-Y. Chiu, A. Grill and P. Avouris, Science **327** (5966), 662 (2010).
12. X. Li, H. Zhu, K. Wang, A. Cao, J. Wei, C. Li, Y. Jia, Z. Li, X. Li and D. Wu, Advanced materials **22** (25), 2743-2748 (2010); B. Xia, Y. Yan, X. Wang and X. W. Lou, Materials Horizons 1 (4), 379-399 (2014).
13. P. R. Wallace, Physical Review **71** (9), 622-634 (1947).
14. A. H. Castro Neto, F. Guinea, N. M. R. Peres, K. S. Novoselov and A. K. Geim, Reviews of Modern Physics **81** (1), 109-162 (2009).
15. G. W. Semenoff, Physical Review Letters **53** (26), 2449-2452 (1984).
16. R. R. Nair, P. Blake, A. N. Grigorenko, K. S. Novoselov, T. J. Booth, T. Stauber, N. M. R. Peres and A. K. Geim, Science **320** (5881), 1308 (2008).
17. P. Blake, P. D. Brimicombe, R. R. Nair, T. J. Booth, D. Jiang, F. Schedin, L. A. Ponomarenko, S. V. Morozov, H. F. Gleeson, E. W. Hill, A. K. Geim and K. S. Novoselov, Nano letters **8** (6), 1704-1708 (2008).
18. A. Reina, X. Jia, J. Ho, D. Nezich, H. Son, V. Bulovic, M. S. Dresselhaus and J. Kong, Nano letters **9** (1), 30-35 (2008).
19. X. Li, Y. Zhu, W. Cai, M. Borysiak, B. Han, D. Chen, R. D. Piner, L. Colombo and R. S. Ruoff, Nano letters **9** (12), 4359-4363 (2009).
20. X. Li, W. Cai, J. An, S. Kim, J. Nah, D. Yang, R. Piner, A. Velamakanni, I. Jung, E. Tutuc, S. K. Banerjee, L. Colombo and R. S. Ruoff, Science **324** (5932), 1312-1314 (2009).
21. H. Bi, F. Huang, J. Liang, X. Xie and M. Jiang, Advanced materials **23** (28), 3202-3206 (2011).
22. Q. Yu, L. A. Jauregui, W. Wu, R. Colby, J. Tian, Z. Su, H. Cao, Z. Liu, D. Pandey, D. Wei, T. F. Chung, P. Peng, N. P. Guisinger, E. A. Stach, J. Bao, S.-S. Pei and Y. P. Chen, Nature materials **10** (6), 443-449 (2011).
23. S. Y. Jeong, S. H. Kim, J. T. Han, H. J. Jeong, S. Yang and G.-W. Lee, ACS Nano **5** (2), 870-878 (2011).
24. H. A. Becerril, J. Mao, Z. Liu, R. M. Stoltenberg, Z. Bao and Y. Chen, ACS Nano **2** (3), 463-470 (2008).
25. S. Gilje, S. Han, M. Wang, K. L. Wang and R. B. Kaner, Nano letters **7** (11), 3394-3398 (2007).
26. X. Wang, L. Zhi and K. Mullen, Nano letters **8** (1), 323-327 (2007).
27. V. C. Tung, M. J. Allen, Y. Yang and R. B. Kaner, Nat Nano **4** (1), 25-29 (2009).
28. G. Eda, G. Fanchini and M. Chhowalla, Nat Nano **3** (5), 270-274 (2008).
29. S. Bae, H. Kim, Y. Lee, X. Xu, J.-S. Park, Y. Zheng, J. Balakrishnan, T. Lei, H. Ri Kim, Y. I. Song, Y.-J. Kim, K. S. Kim, B. Ozyilmaz, J.-H. Ahn, B. H. Hong and S. Iijima, Nat Nano **5** (8), 574-578 (2010).
30. Q. Zheng, W. H. Ip, X. Lin, N. Yousefi, K. K. Yeung, Z. Li and J.-K. Kim, ACS Nano **5** (7), 6039-6051 (2011).
31. I. Khrapach, F. Withers, T. H. Bointon, D. K. Polyushkin, W. L. Barnes, S. Russo and M. F. Craciun, Advanced materials **24** (21), 2844-2849 (2012).
32. K. Kim, H. J. Park, B.-C. Woo, K. J. Kim, G. T. Kim and W. S. Yun, Nano letters **8** (10), 3092-3096 (2008).

33. I. N. Kholmanov, C. W. Magnuson, A. E. Aliev, H. Li, B. Zhang, J. W. Suk, L. L. Zhang, E. Peng, S. H. Mousavi, A. B. Khanikaev, R. Piner, G. Shvets and R. S. Ruoff, Nano letters **12** (11), 5679-5683 (2012).
34. G. Giovannetti, P. Khomyakov, G. Brocks, V. Karpan, J. van den Brink and P. Kelly, Physical Review Letters **101** (2) (2008).
35. Q. Ran, M. Gao, X. Guan, Y. Wang and Z. Yu, Applied Physics Letters **94** (10), 103511 (2009).
36. K. T. Chan, J. B. Neaton and M. L. Cohen, Physical Review B **77** (23), 235430 (2008).
37. E. Watanabe, A. Conwill, D. Tsuya and Y. Koide, Diamond and Related Materials **24** (0), 171-174 (2012).
38. E. J. Lee, K. Balasubramanian, R. T. Weitz, M. Burghard and K. Kern, Nature nanotechnology **3** (8), 486-490 (2008).
39. A. Venugopal, L. Colombo and E. M. Vogel, Applied Physics Letters **96** (1), 013512 (2010).
40. F. Xia, V. Perebeinos, Y.-m. Lin, Y. Wu and P. Avouris, Nat Nano **6** (3), 179-184 (2011).
41. P. A. Khomyakov, G. Giovannetti, P. C. Rusu, G. Brocks, J. van den Brink and P. J. Kelly, Physical Review B **79** (19) (2009).
42. B. Huard, N. Stander, J. Sulpizio and D. Goldhaber-Gordon, Physical Review B **78** (12) (2008).
43. X. Ji, J. Zhang, Y. Wang, H. Qian and Z. Yu, Physical Chemistry Chemical Physics **15** (41), 17883-17886 (2013).
44. Tongay, S., Lemaitre, M., Miao, X., Gila, B., Appleton, B. R., & Hebard, A. F. Physical Review X, 2(1), 011002(2012).
45.S. Tongay, M. Lemaitre, T. Schumann, K. Berke, B. R. Appleton, B. Gila and A. F. Hebard, Applied Physics Letters **99** (10), 102102 (2011).
46. H. Zhong, Z. Liu, G. Xu, Y. Fan, J. Wang, X. Zhang, L. Liu, K. Xu and H. Yang, Applied Physics Letters **100** (12), 122108 (2012).
47. L. Wang, Y. Zhang, X. Li, E. Guo, Z. Liu, X. Yi, H. Zhu and G. Wang, RSC Advances **3** (10), 3359 (2013).
48. S. Kurtin, T. C. McGill and C. A. Mead, Physical Review Letters **22** (26), 1433-1436 (1969).
49. L. F. Lester, J. M. Brown, J. C. Ramer, L. Zhang, S. D. Hersee and J. C. Zolper, Applied Physics Letters **69** (18), 2737 (1996).
50. S. M. Sze and K. K.Ng, in physics of semiconductor devices, 3rd ed. (Wiley, Hoboken, 2007).
51. Y.-J. Yu, Y. Zhao, S. Ryu, L. E. Brus, K. S. Kim and P. Kim, Nano letters **9** (10), 3430-3434 (2009).
52. C. Y. Su, D. Fu, A. Y. Lu, K. K. Liu, Y. Xu, Z. Y. Juang and L. J. Li, Nanotechnology **22** (18), 185309 (2011).
53. R. T. Tung, Physical Review B **64** (20), 205310 (2001).
54. R. T. Tung, Materials Science and Engineering: R: Reports **35** (1–3), 1-138 (2001).
55. R. Tung, Physical Review B **64** (20) (2001).
56. C. Gong, D. Hinojos, W. Wang, N. Nijem, B. Shan, R. M. Wallace, K. Cho and Y. J. Chabal, ACS Nano **6** (6), 5381-5387 (2012).
57. L. S. Yu, Q. Z. Liu, Q. J. Xing, D. J. Qiao, S. S. Lau and J. Redwing, Journal of Applied Physics **84** (4), 2099 (1998).
58. G. Gomila, O. M. Bulashenko and J. M. Rubí, Journal of Applied Physics **83** (5), 2619 (1998).
59. X. A. Cao, E. B. Stokes, P. M. Sandvik, S. F. LeBoeuf, J. Kretchmer and D. Walker, Electron Device Letters, IEEE **23** (9), 535-537 (2002).
60. T. Metzger, R. Höpler, E. Born, O. Ambacher, M. Stutzmann, R. Stömmer, M. Schuster, H. Göbel, S. Christiansen, M. Albrecht and H. P. Strunk, Philosophical Magazine A **77** (4), 1013-1025 (1998).
61. X. Li, L. Fan, Z. Li, K. Wang, M. Zhong, J. Wei, D. Wu and H. Zhu, Advanced Energy Materials **2** (4), 425-429 (2012).
62. E. Shi, H. Li, L. Yang, L. Zhang, Z. Li, P. Li, Y. Shang, S. Wu, X. Li, J. Wei, K. Wang, H. Zhu, D. Wu, Y. Fang and A. Cao, Nano letters **13** (4), 1776-1781 (2013).
63. S. Chandramohan, J. H. Kang, B. D. Ryu, J. H. Yang, S. Kim, H. Kim, J. B. Park, T. Y. Kim, B. J. Cho, E. K. Suh and C. H. Hong, ACS applied materials & interfaces **5** (3), 958-964 (2013).
64. DasA, PisanaS, ChakrabortyB, PiscanecS, S. K. Saha, U. V. Waghmare, K. S. Novoselov, H. R. Krishnamurthy, A. K. Geim, A. C. Ferrari and A. K. Sood, Nat Nano **3** (4), 210-215 (2008).
65. W. J. R. Hoefer, Microwave Theory and Techniques, IEEE Transactions on **33** (10), 882-893

(1985).
66. L. Wang, Y. Zhang, X. Li, Z. Liu, E. Guo, X. Yi, J. Wang, H. Zhu and G. Wang, Journal of Physics D: Applied Physics **45** (50), 505102 (2012).
67. L. Wang, Z. Liu, E. Guo, H. Yang, X. Yi and G. Wang, ACS applied materials & interfaces **5** (12), 5797-5803 (2013).
68. H.-M. Huang, C.-Y. Chang, Y.-S. Hsu, T.-C. Lu, Y.-P. Lan and W.-C. Lai, Applied Physics Letters **101** (6), 061905 (2012).
69. G. Jo, M. Choe, C. Y. Cho, J. H. Kim, W. Park, S. Lee, W. K. Hong, T. W. Kim, S. J. Park, B. H. Hong, Y. H. Kahng and T. Lee, Nanotechnology **21** (17), 175201 (2010).
70. T. H. Seo, T. S. Oh, S. J. Chae, A. H. Park, K. J. Lee, Y. H. Lee and E.-K. Suh, Japanese Journal of Applied Physics **50**, 125103 (2011).
71. B.-J. Kim, C. Lee, Y. Jung, K. Hyeon Baik, M. A. Mastro, J. K. Hite, C. R. Eddy and J. Kim, Applied Physics Letters **99** (14), 143101 (2011).
72. B.-J. Kim, M. A. Mastro, J. Hite, C. R. Eddy and J. Kim, Opt. Express **18** (22), 23030-23034 (2010).
73. B.-J. Kim, G. Yang, M. Joo Park, J. Seop Kwak, K. Hyeon Baik, D. Kim and J. Kim, Applied Physics Letters **102** (16), 161902 (2013).
74. J.-P. Shim, T. Hoon Seo, J.-H. Min, C. Mo Kang, E.-K. Suh and D.-S. Lee, Applied Physics Letters **102** (15), 151115 (2013).
75. Y. Zhang, X. Li, L. Wang, X. Yi, D. Wu, H. Zhu and G. Wang, Nanoscale **4** (19), 5852-5855 (2012).
76. T. H. Seo, K. J. Lee, T. S. Oh, Y. S. Lee, H. Jeong, A. H. Park, H. Kim, Y. R. Choi, E.-K. Suh, T. V. Cuong, V. H. Pham, J. S. Chung and E. J. Kim, Applied Physics Letters **98** (25), 251114 (2011).
77. X. Kun, X. Chen, D. Jun, Z. Yanxu, G. Weiling, M. Mingming, Z. Lei and S. Jie, Applied Physics Letters **102** (16), 162102 (2013).
78. P. Kumar, L. S. Panchakarla, S. V. Bhat, U. Maitra, K. S. Subrahmanyam and C. N. Rao, Nanotechnology **21** (38), 385701 (2010).
79. J. Min Lee, J. Yi, W. Woo Lee, H. Yong Jeong, T. Jung, Y. Kim and W. Il Park, Applied Physics Letters **100** (6), 061107 (2012).
80. T. H. Seo, A. H. Park, G. H. Lee, M. J. Kim and E.-K. Suh, Journal of Physics D: Applied Physics 47 (31), 315102 (2014).
81. J. P. Shim, D. Kim, M. Choe, T. Lee, S. J. Park and D. S. Lee, Nanotechnology **23** (25), 255201 (2012).
82. T. Hoon Seo, B. Kyoung Kim, G. Shin, C. Lee, M. Jong Kim, H. Kim and E.-K. Suh, Applied Physics Letters **103** (5), 051105 (2013).
83. Z. Li, J. Kang, Z. Liu, C. Du, X. Lee, X. Li, L. Wang, X. Yi, H. Zhu and G. Wang, AIP Advances **3** (4), 042134 (2013).
84. M. Choe, C.-Y. Cho, J.-P. Shim, W. Park, S. K. Lim, W.-K. Hong, B. Hun Lee, D.-S. Lee, S.-J. Park and T. Lee, Applied Physics Letters **101** (3), 031115 (2012).
85. T. H. Seo, S. J. Chae, B. K. Kim, G. Shin, Y. H. Lee and E.-K. Suh, Applied Physics Express **5** (11), 115101 (2012).
86. C.-Y. Cho, M. Choe, S.-J. Lee, S.-H. Hong, T. Lee, W. Lim, S.-T. Kim and S.-J. Park, Journal of Applied Physics **113** (11), 113102 (2013).
87. H. Liu, Y. Liu and D. Zhu, Journal of Materials Chemistry **21** (10), 3335 (2011).
88. Y. Shi, K. K. Kim, A. Reina, M. Hofmann, L.-J. Li and J. Kong, ACS Nano **4** (5), 2689-2694 (2010).
89. A. Kasry, M. A. Kuroda, G. J. Martyna, G. S. Tulevski and A. A. Bol, ACS Nano **4** (7), 3839-3844 (2010).
90. S. Chandramohan, J. Hye Kang, Y. S. Katharria, N. Han, Y. Seon Beak, K. Bok Ko, J. Bae Park, H. Kyu Kim, E.-K. Suh and C.-H. Hong, Applied Physics Letters **100** (2), 023502 (2012).
91. S. Chandramohan, J. H. Kang, Y. S. Katharria, N. Han, Y. S. Beak, K. B. Ko, J. B. Park, B. D. Ryu, H. K. Kim, E.-K. Suh and C.-H. Hong, Journal of Physics D: Applied Physics **45** (14), 145101 (2012).
92. L. Wang, Y. Zhang, X. Li, Z. Liu, L. Zhang, E. Guo, X. Yi, H. Zhu and G. Wang, Proceedings of the Royal Society A: Mathematical, Physical and Engineering Sciences **469** (2151), 20120652-20120652 (2013).
93. L. Wang, Y. Zhang, X. Li, Z. Liu, E. Guo, X. Yi, J. Wang, H. Zhu and G. Wang, Applied Physics

Letters **101** (6), 061102 (2012).
94. R. H. Kim, M. H. Bae, D. G. Kim, H. Cheng, B. H. Kim, D. H. Kim, M. Li, J. Wu, F. Du, H. S. Kim, S. Kim, D. Estrada, S. W. Hong, Y. Huang, E. Pop and J. A. Rogers, Nano letters **11** (9), 3881-3886 (2011).
95. J. Kang, Z. Li, H. Li, Z. Liu, X. Li, X. Yi, P. Ma, H. Zhu and G. Wang, Applied Physics Express **6** (7), 072102 (2013); L. Wang, J. Ma, Z. Liu, X. Yi, H. Zhu and G. Wang, ACS Photonics, DOI:10.1021/ph500133w.
96. C. H. Lee, Y. J. Kim, Y. J. Hong, S. R. Jeon, S. Bae, B. H. Hong and G. C. Yi, Advanced materials **23** (40), 4614-4619 (2011).
97. N. Han, T. V. Cuong, M. Han, B. D. Ryu, S. Chandramohan, J. B. Park, J. H. Kang, Y. J. Park, K. B. Ko, H. Y. Kim, H. K. Kim, J. H. Ryu, Y. S. Katharria, C. J. Choi and C. H. Hong, Nature communications **4**, 1452 (2013).
98. K. Chung, C. H. Lee and G. C. Yi, Science **330** (6004), 655-657 (2010).
99. Y. Zhang, L. Wang, X. Li, X. Yi, N. Zhang, J. Li, H. Zhu and G. Wang, Journal of Applied Physics **111** (11), 114501 (2012).
100. L. L. Chang, Applied Physics Letters **24** (12), 593 (1974).
101. K. Joo, S. K. Jerng, Y. S. Kim, B. Kim, S. Moon, D. Moon, G. D. Lee, Y. K. Song, S. H. Chun and E. Yoon, Nanotechnology **23** (42), 425302 (2012).
102. S. P. Koenig, N. G. Boddeti, M. L. Dunn and J. S. Bunch, Nat Nano **6** (9), 543-546 (2011).
103. T. Yoon, W. C. Shin, T. Y. Kim, J. H. Mun, T. S. Kim and B. J. Cho, Nano letters **12** (3), 1448-1452 (2012).
104. C. Mattevi, H. Kim and M. Chhowalla, Journal of Materials Chemistry **21** (10), 3324-3334 (2011).
105. K. S. Kim, Y. Zhao, H. Jang, S. Y. Lee, J. M. Kim, K. S. Kim, J. H. Ahn, P. Kim, J. Y. Choi and B. H. Hong, Nature **457** (7230), 706-710 (2009).
106. A. Grüneis, K. Kummer and D. V. Vyalikh, New Journal of Physics **11** (7), 073050 (2009).
107. M. Zheng, K. Takei, B. Hsia, H. Fang, X. Zhang, N. Ferralis, H. Ko, Y.-L. Chueh, Y. Zhang, R. Maboudian and A. Javey, Applied Physics Letters **96** (6), 063110 (2010).
108. A. T N'Diaye, M. Engler, C. Busse, D. Wall, N. Buckanie, F.-J. Meyer zu Heringdorf, R. van Gastel, B. Poelsema and T. Michely, New Journal of Physics **11** (2), 023006 (2009).
109. T. Aizawa, R. Souda, S. Otani, Y. Ishizawa and C. Oshima, Physical Review Letters **64** (7), 768-771 (1990).
110. Z. Peng, Z. Yan, Z. Sun and J. M. Tour, ACS Nano **5** (10), 8241-8247 (2011).
111. Z. Yan, Z. Peng, Z. Sun, J. Yao, Y. Zhu, Z. Liu, P. M. Ajayan and J. M. Tour, ACS Nano **5** (10), 8187-8192 (2011).
112. S. Jie, E. Lind, I. Maximov and H. Q. Xu, Electron Device Letters, IEEE **32** (2), 131-133 (2011).
113. J. Sun, M. Larsson, I. Maximov and H. Q. Xu, Applied Physics Letters **96** (16), 162107 (2010).
114. J. Sun, M. T. Cole, N. Lindvall, K. B. K. Teo and A. Yurgens, Applied Physics Letters **100** (2), 022102 (2012).
115. J. Sun, N. Lindvall, M. T. Cole, T. Wang, T. J. Booth, P. Bøggild, K. B. K. Teo, J. Liu and A. Yurgens, Journal of Applied Physics **111** (4), 044103 (2012).
116. J. Sun, N. Lindvall, M. T. Cole, K. B. K. Teo and A. Yurgens, Applied Physics Letters **98** (25), 252107 (2011).
117. M. H. Rümmeli, A. Bachmatiuk, A. Scott, F. Börrnert, J. H. Warner, V. Hoffman, J.-H. Lin, G. Cuniberti and B. Büchner, ACS Nano **4** (7), 4206-4210 (2010).
118. A. Scott, A. Dianat, F. Börrnert, A. Bachmatiuk, S. Zhang, J. H. Warner, E. Borowiak-Paleń, M. Knupfer, B. Büchner, G. Cuniberti and M. H. Rümmeli, Applied Physics Letters **98** (7), 073110 (2011).
119. D. Ehrentraut, E. Meissner, M. Bockowski, <<Technology of Gallium Nitride Crystal Growth>>,springer.
120. J.-i. Fujita, R. Ueki, Y. Miyazawa and T. Ichihashi, Journal of Vacuum Science & Technology B: Microelectronics and Nanometer Structures **27** (6), 3063 (2009).
121. H. Hiura, M. V. Lee, A. V. Tyurnina and K. Tsukagoshi, Carbon **50** (14), 5076-5084 (2012).
122. J. Sun, M. T. Cole, S. A. Ahmad, O. Backe, T. Ive, M. Loffler, N. Lindvall, E. Olsson, K. B. K. Teo,

L. Johan, A. Larsson, A. Yurgens and A. Haglund, Semiconductor Manufacturing, IEEE Transactions on **25** (3), 494-501 (2012).
123. B.-J. Kim, C. Lee, M. A. Mastro, J. K. Hite, C. R. Eddy, F. Ren, S. J. Pearton and J. Kim, Applied Physics Letters 101 (3), - (2012).
124. L. Liu, S. Ryu, M. R. Tomasik, E. Stolyarova, N. Jung, M. S. Hybertsen, M. L. Steigerwald, L. E. Brus and G. W. Flynn, Nano Letters 8 (7), 1965-1970 (2008).
125. S. Rumyantsev, G. Liu, W. Stillman, M. Shur and A. A. Balandin, Journal of Physics: Condensed Matter 22 (39), 395302 (2010).
126. Z. Liu, A. A. Bol and W. Haensch, Nano Letters 11 (2), 523-528 (2010).
127. M. R. Choudhury, Y. Youngki, J. Guo and K. Mohanram, Nanotechnology, IEEE Transactions on 10 (4), 727-736 (2011).
128. Y. Tianhua, L. Eun-Kyu, B. Briggs, B. Nagabhirava and Y. Bin, Electron Device Letters, IEEE 31 (10), 1155-1157 (2010).
129. Y. Tianhua, L. Eun-Kyu, B. Briggs, B. Nagabhirava and Y. Bin, Nanotechnology, IEEE Transactions on 10 (4), 710-714 (2011).

Figures and tables captions

Fig. 1: (a) shows the band structure of graphene (left) and zoom-in of the energy bands close to one of the Dirac points (right)[14]; (b1) shows the transmittances of single layer (SLG) (~97.7%) and bilayer graphene (~95.4%)[16]; (b2) shows the transmittance of graphene versus light wavelength (400-2500nm);[16] Inset of (b2) shows the transmittances of white light as a function of the number of graphene layers[16]; (c) summarizes the sheet resistance and optical transmission for graphene TCEs reported from different groups.

Fig. 2: (a1) and (b1) show the schematic drawing of lateral and vertical LED devices with graphene TCEs; (c1) and (c2) show the sketch band diagram of graphene/p-GaN junction before and after alignment; (d1) and (d2) show the schematic band structures and carriers transportation when graphene contacts with p-GaN and n-GaN.

Fig. 3: (a) sketch of the principle of interface engineering approach for graphene TCEs utilization: metal (Au, Ag, Ni) and ITO dot, NW and ultra-thin film are inserted between graphene TCEs and p-GaN; (b1) schematic diagram of the position of the Dirac point and the Fermi level as a function of doping. The upper panel is n-type doped, pristine and p type doped free standing graphene (a to c) [87]. The lower panel is n-type doped, pristine and p-type doped graphene grown on silicon carbide (SiC) (d to f); (b2) shows the experimental set up for HNO3[47,92] evaporation graphene doping; (b3) summarized decrease of sheet resistance by using various wet doping agents [29].

Fig. 4: (a) sketches the tunnel junction LED device design for graphene TCEs; (b) sketches n-$(In)_xGa_{1-x}N$/p-GaN band diagram; (c1) shows the top-view SEM images of LED chip after transferring graphene; (c2) shows the I-V curves and I-LOP of LEDs based on conventional ITO, bare graphene and graphene-InGaN TCEs.

Fig. 5: (a) micrograph of exfoliated wet-transferred graphene (with PMMA) on GaN

substrate; (b) sketches the growth mechanism of graphene on GaN; (c1 up)[121] Carbon thin films on GaN/sapphire (left two) and the bare substrate (right), (c1 lower) High-resolution cross-section TEM micrograph of a carbon/GaN sample, where the carbon thin film is intentionally grown thicker for easy detection of the graphitic layers; (c2) UV-VIS-NIR transmittance of the carbon thin film and the bare GaN/sapphire. The carbon thin film absorbs ~2% of the incident light. Insert: FTIR spectra of the same samples, which have been shifted along the ordinate for clarity; (c3) Raman spectra (514nm, 0.5mW) of the as-grown carbon thin film on GaN.

Table. 1 (a) Two categories of metal contact with graphene; (b) summarize the obtained Ψ_b by different groups and different methods;

Table. 2 list the reported interface engineered graphene hybrid structure, feature and its correspondent chip results.

Table. 3 list the electrical and optical characteristics of blue and near ultra-violet LEDs with Au-doped graphene TCE-based LED.

Fig. 1

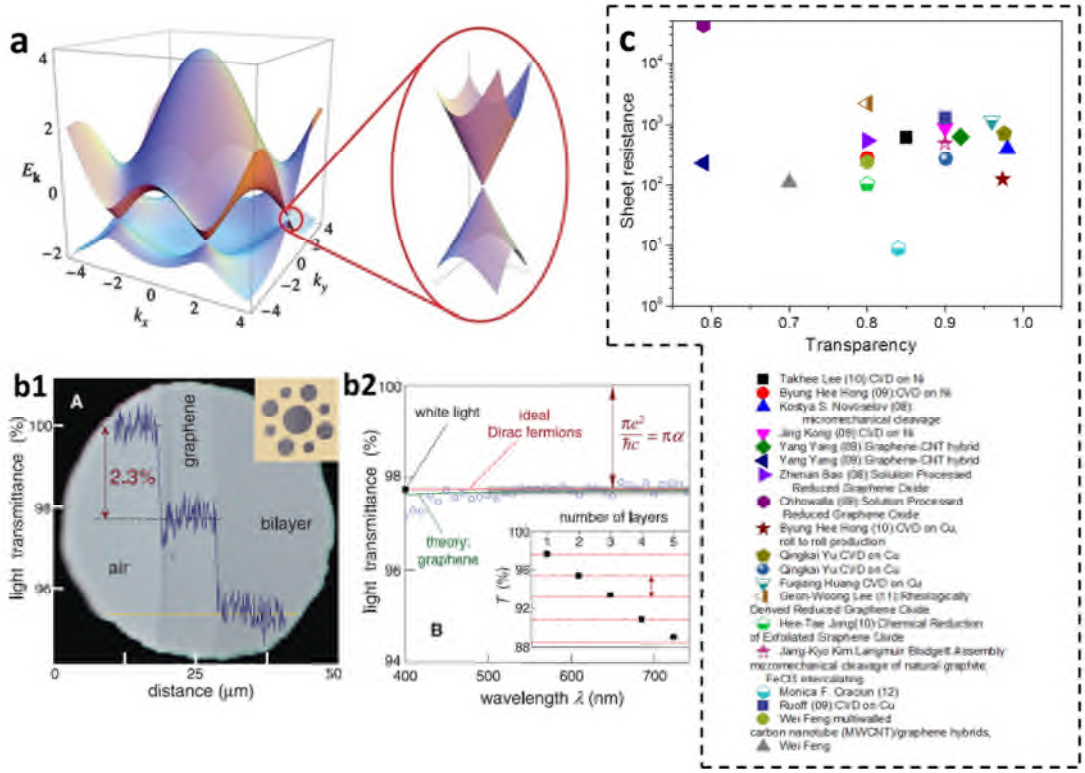
a
E_k
k_x
k_y
c
Sheet resistance
Transparency
b1
A
graphene
bilayer
air
2.3%
light transmittance (%)
distance (μm)
b2
white light
ideal
Dirac fermions
$\frac{\pi e^2}{\hbar c} = \pi\alpha$
theory: graphene
number of layers
B
light transmittance (%)
wavelength λ (nm)
Takhee Lee (10) CVD on Ni
Byung Hee Hong (09) CVD on Ni
Kostya S. Novoselov (08) micromechanical cleavage
Jing Kong (09) CVD on Ni
Yang Yang (09) Graphene-CNT hybrid
Yang Yang (09) Graphene-CNT hybrid
Zhenan Bao (08) Solution Processed Reduced Graphene Oxide
Chihwalla (09) Solution Processed Reduced Graphene Oxide
Byung Hee Hong (10) CVD on Cu, roll to roll production
Qingkai Yu CVD on Cu
Qingkai Yu CVD on Cu
Fuqiang Huang CVD on Cu
Geon-Woong Lee (11) Rheologically Derived Reduced Graphene Oxide
Hee-Tae Jung (10) Chemical Reduction of Exfoliated Graphene Oxide
Jang-Kyo Kim Langmuir Blodgett Assembly micromechanical cleavage of natural graphite
FeCl3 intercalating
Monica F. Craciun (12)
Ruoff (09) CVD on Cu
Wei Feng multiwalled carbon nanotube (MWCNT)/graphene hybrids,
Wei Feng

Fig. 2

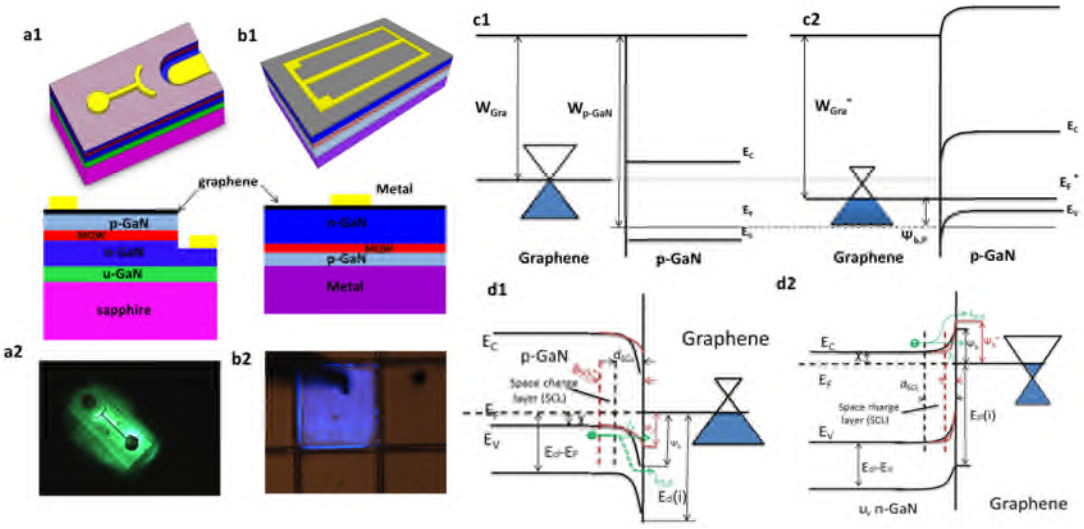
a1
b1
graphene
Metal
p-GaN
MQW
n-GaN
u-GaN
sapphire
n-GaN
MQW
p-GaN
Metal
a2
b2
c1
c2
W_{Gra}
$W_{p\text{-}GaN}$
E_C
E_F
E_V
Graphene
p-GaN
W_{Gra}^*
E_F^*
$\Psi_{b,P}$
d1
d2
E_C
p-GaN
Graphene
Space charge layer (SCL)
E_F
E_V
E_D-E_F
E_D(i)
u, n-GaN

Fig. 3

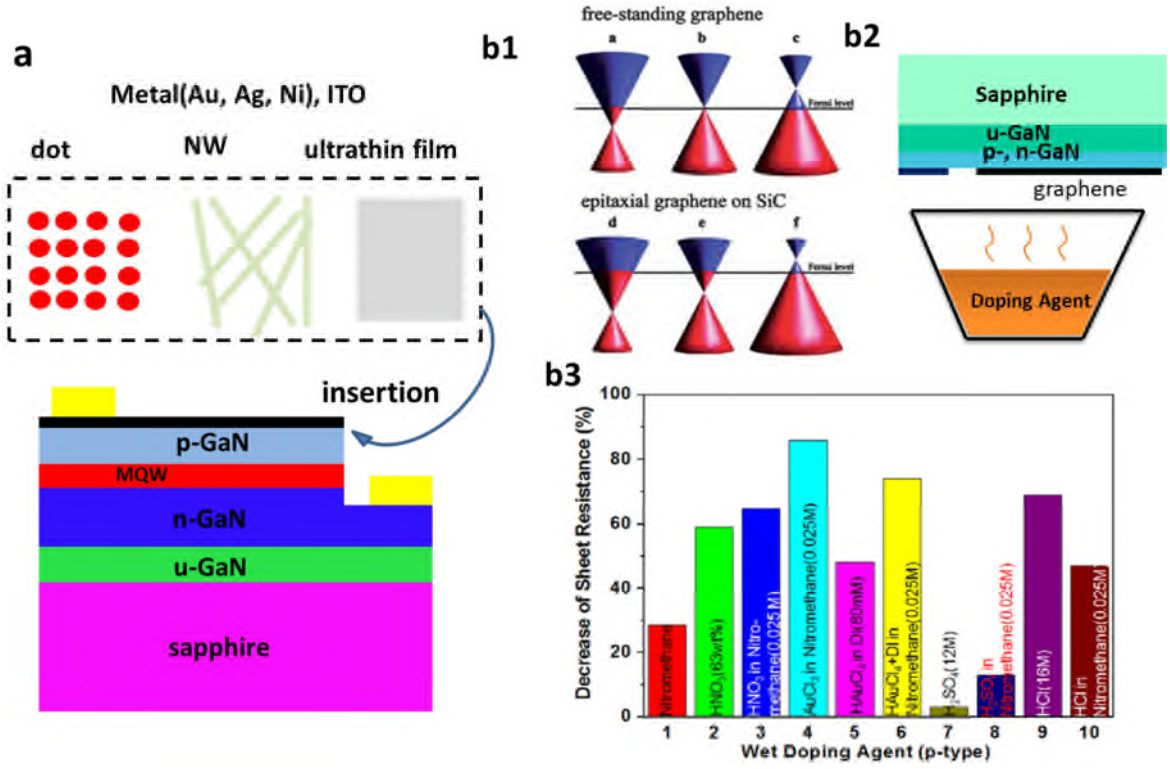
a
Metal(Au, Ag, Ni), ITO
dot
NW
ultrathin film
insertion
p-GaN
MQW
n-GaN
u-GaN
sapphire
b1
free-standing graphene
epitaxial graphene on SiC
b2
Sapphire
u-GaN
p-, n-GaN
graphene
Doping Agent
b3
Decrease of Sheet Resistance (%)
Wet Doping Agent (p-type)
Nitromethane
HNO3 (65wt%)
HNO3 in Nitromethane(0.025M)
AuCl3 in Nitromethane(0.025M)
HAuCl4 in DI(80mM)
HAuCl4+DI in Nitromethane(0.025M)
H2SO4(12M)
HCl(16M)
HCl in Nitromethane(0.025M)

Fig. 4

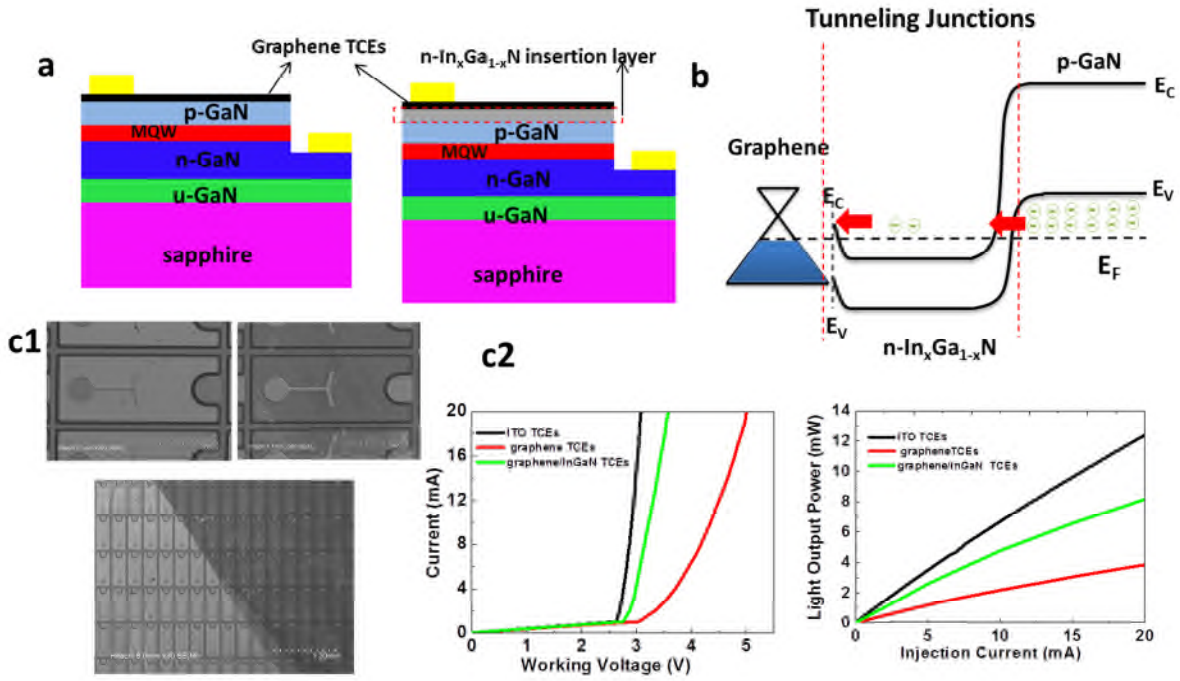
a
Graphene TCEs
n-In$_x$Ga$_{1-x}$N insertion layer
p-GaN
MQW
n-GaN
u-GaN
sapphire
b
Tunneling Junctions
p-GaN
Graphene
E_C
E_V
E_F
n-In$_x$Ga$_{1-x}$N
c1
c2
ITO TCEs
graphene TCEs
graphene/InGaN TCEs
Current (mA)
Working Voltage (V)
Light Output Power (mW)
Injection Current (mA)

Fig. 5

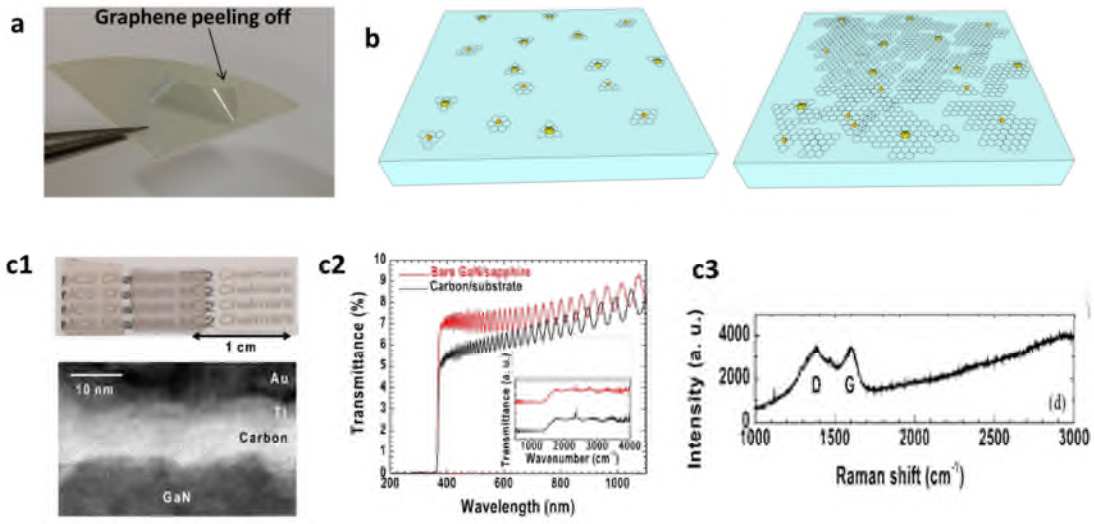
a
Graphene peeling off
b
c1
1 cm
10 nm
Au
Ti
Carbon
GaN
c2
Bare GaN/sapphire
Carbon/substrate
Transmittance (%)
Wavelength (nm)
Transmittance (a. u.)
Wavenumber (cm-1)
c3
Intensity (a. u.)
D
G
(d)
Raman shift (cm-1)

Fig. S1

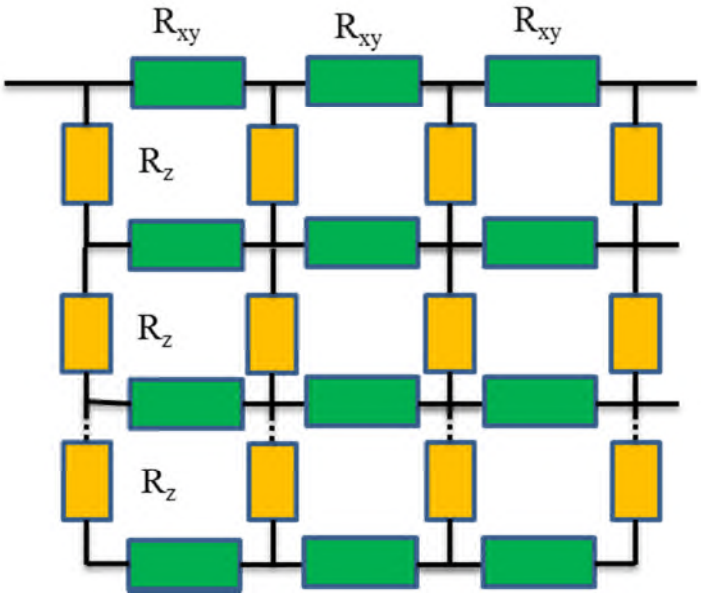

Table .1

(a)

strong contact metal	Ni, Co, Pd, Ti, Cr
weak contact metal	Al, Ag, Cu, Au, Pt, Ir, Ga

(b)

	Theoretically predicted value (Ψ_b^T)	**S. Tongay group**	**Haijian Zhong group**	**Our group**	
				I-V fitting (Ψ_b^F)	**XPS (Ψ_b^X)**
graphene/n-GaN	0.7	0.73	0.33±0.01	0.36±0.01	0.57
graphene/p-GaN	2.7	N A	0.36±0.01	0.49±0.02	2.08
graphene/n-Si	0.75	0.86	N A	0.78	N A
graphene/n-GaAs	0.7	0.79	N A		

Table. 2

TCEs structure	TCEs feature			Chip feature	ρ_c (Ωcm^2)	Chip Characterization	
		T	Rs(Ω/sq)				
AgNWs/ Gra (with different AgNWs concentration) [83]	0.1mg/ml	96.7%	801	177.8*228.6μm^2; 460nm	Gra /p-GaN:1.06; Gra /AgNWs/p-GaN:1.05*10^{-1}	Gra/AgNWs: 8.4V,7.8V,6.6V@20mA, respectively; Bare Gra: 11.8V@20mA	
	0.5 mg/ml	96%;	645				
	1.0mg/ml	92.8%	367				
AgNWs/Gra[82]	AgNWs/Gra	86.3%	500±100	350*350μm^2 UV(375nm)	NA	Bare Gra: 10.9V@20mA); AgNWs: 6.7V@20mA; AgNWs/Gra: 4.48V@20mA; 250% EL improvement (AgNWs/Gra compared with bare gra)	
	Bare gra	93%	30±3				
ITO dot (7-10nm)/Gra; cold wall rapid CVD growth[77]	Single Gra	96.7%@ 460nm; (88.2% @320nm)	800-1000	254*254μm^2	NA	Bare Gra: 6.76V@20mA; ITOdot/Gra: 3.9V@20mA; Conventional ITO:3.6V@20mA;	
	MItilayer Gra	91.7%@460nm; (81.9%@320nm)	300-350				
NiOx(1nm)/Gra [75]	T=90%			225*175μm^2	Gra /NiOx/p-GaN: 5.9 *10^{-4}	@20mA:3.65V(Gra/NiOx);6.15V(bare Gra);3.2V(ITO)	
NiOx(2nm)/Gra [63]					Gra /NiOx/p-GaN: 8.8*10^{-1}	@20mA:3.16V(Gra/NiOx);4.5V(Bare Gra) Lower output power of Gra/NiOx TCEs;	
Ni/Ag/Gra/ZnO nanorods79	t~70%-80%				0.5	2.5V@0.01mA; 66% EL increased over bare Gra;	
ITO dots /Gra[76]	diameter 150nm, density 3.8*10^9 cm^2 T=85%@550nm; Rs=2.2*10^3					@20mA: 6.4V(bare Gra); 6.1V(ITO dots);3.66V (ITO dots/Gra); 1.5 times LOP increases (ITO dots over bare Gra)	
ITO dots /Gra (Gra grown by Chemical	T~90%			315*315μm^2 UV LED (~380nm)		@20mA: 5.9V (bare Gra); 4.9V (Gra on ITO dots); 4.42V (CCG on ITO dots);4.35V (conventional ITO); EL increases 150% and 60% for CCG/ITO and graphene ITO over conventional ITO, respectively;	
(p-GaN) /Gra/Ni(3nm) [74]	Gra/Ni	75%	690±50	Blue:460nm UV:380nm		Blue	UV
	Gra	90%	1250±50			@20mA:6.2V(bare Gra); 4.8V(Ni/Gra); 3.5V(ITO) 50% decreased EL over ITO;	@20mA;13.2V(Gra); 7.1V(Gra/Ni) 83% EL of ITO;
	ITO	86% @460nm, 70% @380nm	43±5				

Table. 3

Graphene doping agent		TCEs feature			Chip results		
		W_F (eV)	T	R_s	I-V	EL	Peak wavelength
$AuCl_3$[90]	0mM	4.42	89%	1000±698	4.73V@0.4 mA	1	460nm
	5mM	4.77	85%	203±37	3.94V@0.4mA	1.938	
	20mM	5.12	78%	105±7	3.86V@0.4mA	1.287	
Au nano particle[82]	Bare Gra	NA	88%	1000±100	7.8V@20mA	1	415nm
	Au-Gra	NA	88%	18±2	6.8V@20mA	1.34	